Exploitation of the Secretory Pathway by SARS-CoV-2 Envelope

Guy J Pearson[1,2], Malgorzata Broncel[3], Ambrosius P Snijders[3] and Jeremy G Carlton[1,2]*

1. School of Cancer and Pharmaceutical Sciences, King's College London, SE1 1UL, UK
2. Organelle Dynamics Laboratory, The Francis Crick Institute, 1 Midland Road, London, NW1 1AT, UK
3. Proteomics Science Technology Platform, The Francis Crick Institute, 1 Midland Road, NW1 1AT, UK.

*Correspondence to: Jeremy.Carlton@kcl.ac.uk

Abstract

The beta-coronavirus SARS-CoV-2 is the causative agent of the current global COVID-19 pandemic. Coronaviruses are enveloped RNA viruses. Assembly and budding of coronavirus particles occur at the Endoplasmic Reticulum-Golgi Intermediate Compartment (ERGIC), with the structural proteins Nucleocapsid, Spike, Membrane and Envelope facilitating budding and release of virions into the secretory pathway lumen. This allows viral release which can occur through delivery of virus particles to deacidified lysosomes and subsequent lysosomal secretion. Coronaviral Envelope proteins are necessary for coronavirus assembly, play important roles in replication and can form oligomeric cation channels. Whilst synthesised in the ER, the mechanism by which Envelope achieves its steady state localisation to the ERGIC remains unclear. Here, we used fluorescent reporters to illuminate the Envelope protein from SARS-CoV-2. We discovered that internal tagging of this protein is necessary to preserve the functionality of a C-terminal ER-export motif and to allow localisation of Envelope to the ERGIC. Using this non-disruptive form of tagging, we used proximity biotinylation to define the vicinal proteome of wild type and ER-restricted versions of Envelope. We show that both Envelope and the presence of its ER-export motif contribute to the packaging of nucleocapsid into virus like particles. Finally, using our labelled versions of Envelope, we discovered that a minor pool of this protein is delivered to lysosomes. We show that lysosomal Envelope is oligomeric and can contribute to pH neutralisation in these organelles.

Introduction

The Severe Acute Respiratory Syndrome Coronavirus-2 (SARS-CoV-2) is the causative agent of the global COVID-19 pandemic. SARS-CoV-2 is an enveloped, beta-coronavirus with a positive-sense, single-stranded RNA genome encoding 29 proteins[1]. Late events in the beta-coronaviral lifecycle are orchestrated by 4 of these proteins, the RNA-binding protein Nucleocapsid (N) and three transmembrane proteins Spike (S), Membrane (M) and Envelope (E). S is a class I transmembrane glycoprotein that is necessary for viral entry[2,3]. M contains three-transmembrane domains and is the most abundant transmembrane in the viral particle[4]. E is a small single pass transmembrane protein that is found as a minor component of viral particles and can assemble as a pentameric cation channel[5,6]. Viral assembly occurs at the Endoplasmic Reticulum/Golgi Intermediate Compartment (ERGIC) and involves the budding of nascent S, M and E-containing particles into the ERGIC lumen[7,8]. During this process, newly replicated viral RNA is incorporated into budding virions in complex with N. Virus like particle (VLP) systems represent a minimal system in which to study virion assembly, and have demonstrated that M and E are both necessary and sufficient for particle assembly[9–12] and can package RNAs when N is present[10]. Once virus particles have been released into the secretory pathway, exposed sequences can be post-translationally modified and virions can egress from cells as luminal content. Whilst the canonical secretory pathway was assumed to be the egress route, recent data suggest that beta-coronaviruses can be delivered to deacidified lysosomes for atypical secretion via lysosomal exocytosis[13]. The mechanism by which lysosomal function is compromised in these infected cells is unclear, but may involve manipulation of HOPS-dependent lysosomal fusion by SARS-CoV-2 accessory proteins such as ORF3a[14,15] or the presence of viroporins in these membranes. Beyond roles in assembly, what role, if any, SARS-CoV-2 E plays in modulating organellar pH remains to be determined.

Main Text

We sought to create tagged versions of SARS-CoV-2 E to understand how this protein achieves its steady-state localisation at sites of particle assembly. Given the localisation of SARS-CoV E to membranes of the ERGIC and *cis*-Golgi[16,17] and the degree of identity between E from SARS-CoV and SARS-CoV-2 (Figure 1A), we were surprised to find SARS-CoV-2 E bearing N- or C-terminal HaloTag (HT) fusions was restricted to the Endoplasmic Reticulum (ER) (Figure 1A, 1B). Positioning within the secretory pathway is governed by a cargo's interaction with cytoplasmic anterograde and retrograde trafficking machineries, most notably coatomer complex-1 and -2. We wondered if addition of tags to SARS-CoV-2 E's extreme termini altered folding or obscured these signals, preventing ER export to the ERGIC and *cis*-Golgi. We inserted HT at three additional positions in the coding sequence and discovered that tag insertion immediately after the transmembrane domain (Site3), or in a region of E's cytoplasmic tail (Site4) allowed steady state localisation of HT-versions of SARS-CoV-2 E to perinuclear structures with Golgi morphology (Figure 1A and 1B). In addition to the predominate perinuclear localisation, these versions of HT-E also decorated vesicular structures suggesting that they had fully cleared the ER and accessed the secretory pathway (Figure 1A and 1B). Placement of the HT at Site2 also prevented anterograde traffic. We confirmed these localisations using mEmerald (Em) in place of HT (Figure S1A and S1B) and given the cell-to-cell variability observed when assessing membrane trafficking phenotypes, we devised a quantitative reporting system to visually depict E's position within the secretory pathway (Figure 1C and Figure S1B). We used a panel of antibodies and fusion proteins to confirm location of E-HT[Site3] to the ERGIC and Golgi (Figure 1D) suggesting that our internally tagged versions of E recapitulate the known localisation of coronaviral E proteins. Intriguingly, we also detected colocalisation of the peripheral puncta of E-HT[Site3] with LAMP1, suggesting that a small pool of E is trafficked to lysosomes (Figure 1D). We also observed limited colocalization with large, but not small, EEA1-decorated puncta (Figure 1D), suggesting that at steady state, a small pool of E engages with the endocytic pathway and can be delivered to lysosomes.

A C-terminal PDZ-ligand is necessary and sufficient for ER export of SARS-CoV-2 E

The C-terminus of SARS-CoV E encodes a PDZ-ligand able to interact with PDZ-domain containing proteins including Syntenin and PALS1. This sequence is conserved in SARS-CoV-2 E (Figure 1A) and we were surprised to find that its deletion restricted both Em and HT versions of SARS-CoV-2 E to the ER (Figure 1E and 1F, Figure 1 Supplement 1C-E). Grafting this PDZ-sequence onto E-HT^{Site5} restored its anterograde traffic (Figure 1G-1I), indicating that this sequence acts as a dominant ER-export motif allowing SARS-CoV-2 E to gain access to the secretory pathway.

C-terminal hydrophobic sequences can act as COP-II binding sequences for ER export. Whilst the C-terminal Valine provided most of the activity relating to anterograde traffic, some SARS-CoV-2 E-Em^{Site3} ΔV still reached the Golgi and full truncation of the PDZ-domain was needed to restrict ER-export (Figure 1 Supplement 1C-1E). Likewise, replacement of the DLLV PDZ-ligand with AAAV or AALL sequences could only partially recover ER-export (Figure 1 Supplement 1C – 1E) suggesting that the context of this hydrophobic terminal residue is important for ER export. Exploration of different classes of PDZ-ligands in this context revealed that a C-terminal hydrophobic residue was not dominant for ER-export, that a variety of class-I and class-II (but not class-III) PDZ domains could substitute for the DLLV sequence, although none were as effective in allowing ER-export as replacement of the DLLV sequence with chimeric C-termini from MHV (strain S) or MERS (Figure 1 Supplement 1F - 1H). These isolated sequences could similarly rescue ER-export when grafted onto the extreme C-terminus of SARS-CoV-2 E-HT^{Site5} (Figure 1H and 1I). The beta-variant of SARS-CoV-2 encodes a P71L mutation in E, proximal to this sequence. We wondered if this mutation influenced ER-export and discovered that whilst SARS-CoV-2 E-Em^{Site3} P71L displayed steady state localisation to the Golgi, a fraction was retained in the ER and its ability to reach post-Golgi vesicles was limited (Figure 1 Supplement 1I and 1J). These data suggesting that the steady state

distribution of E from beta variants of SARS-CoV-2 is shifted earlier in the secretory pathway.

The transmembrane glycoproteins of coronaviruses are heavily post translationally modified[8]. We wondered if SARS-CoV-2 E's positioning within the secretory pathway influenced the degree of these modifications. By immunoprecipitating SARS-CoV-2 E-HT[Site3], we discovered that versions of E that were retained in the ER were O-GlcNAcylated (Figure 1 Supplement 2A) and mapped sites of O-GlcNAcylation to Ser67 and Ser68 in SARS-CoV-2 E's C-terminus (Figure 1 Supplement 2B and 2C).

Envelope localisation to the ERGIC is necessary for Nucleocapsid packaging into VLPs

VLP systems have proved an excellent tool by which to analyse late events in the coronavirus lifecycles and have demonstrated that E and M are necessary and sufficient for particle assembly. Using a 4-component (E, S, M, N) VLP system in 293T cells, we discovered that SARS-CoV-2 M was essential for particle generation, as its omission resulted in a failure to recover N or S in VLP fractions (Figure 2A). Whilst omission of E had only minor effects on the biogenesis of VLPs, we noticed that particles produced in the absence of E contained less N (Figure 2A). We next wondered how restricting E to the ER would impact VLP generation. As with omission of E, we found that E ΔDLLV did not disrupt VLP generation, as M could be similarly recovered from the VLP fraction. However, N incorporation into these VLPs was similarly impaired (Figure 2A). These data suggest that E's C-terminal DLLV motif or the presence of E at the site of particle biogenesis supports N incorporation.

Using proximity biotinylation to reveal the vicinal interactome of SARS-CoV-2 Envelope

We next inserted HA-tagged TurboID, a fast-acting promiscuous biotin ligase[18] into these internal sites. We confirmed steady-state localisation of TurboID versions of E to the ERGIC (Figure 3 Supplement 1A). We used proximity biotinylation, mass spectrometry and label-free quantification to determine proteins vicinal to these

versions of SARS-CoV-2 E (Figure 3A, Supplementary Table 1). Pleasingly, we could recover significant enrichment of ERGIC and Golgi proteins including ERGIC53, GORASP2, a number of Golgi SNAREs (GOSR1, GOSR2, VAMP3) and components of anterograde (SEC24B) and retrograde (RER1) transport mechanisms for HA-TurboID tagged versions of SARS-CoV-2 E (Figure 3A). Whilst we recovered biotinylated peptides from known partners of SARS-CoV-2 E, including TJP1[19], and PALS-1[15,20] (Figure 3A, Supplementary Table 2), we were unable to recover any biotinylated peptides from Syntenin, a previously described binding partner for SARS-CoV E[21]. We confirmed physical interactions with RER1, PALS-1 and GORASP2 by immunoprecipitation of endogenous protein (Figure 3B). We used LFQ to compare vicinal proteomes from Golgi (E-HA-TurboID ^{Slte3} , E-HA-TurboID^{Slte4} and E-HA-TurboID^{Slte3} ΔDLLV + DEWV), ER (E-HA-TurboID^{Slte3} ΔDLLV and E-HA-TurboID^{Site4} ΔDLLV and E-HA-TurboID^{Slte3} ΔDLLV + SVKI) localised versions of SARS-CoV-2 E. Recovered proteomes clustered well and Principle Component Analysis separated both groups from each other and from a cytosolic control (Figure 3 Supplement 1B and 1C). We recovered numerous PDZ-domain containing proteins with WT but not ΔDLLV versions of SARS-CoV-2 E (Figure 3 Supplement 1D, Supplementary Table 3), suggesting that this sequence can act as a PDZ ligand. Analysis of these vicinal proteomes revealed strong enrichment of Golgi and ERGIC proteins for wildtype versions of HA-Turbo ID SARS-CoV-2 E, and strong enrichment of ER-proteins for HA-Turbo ID SARS-CoV-2 E ΔDLLV (Figure 3 Supplement 1E-1G). Consistent with localisation of E-Em^{Site3} to lysosomes (Figure 1D), we discovered that a number of clathrin-adaptor proteins and lysosomal proteins were selectively biotinylated by wild-type versions of SARS-CoV-2 E, but not by versions restricted to the ER (Figure 3 Supplement 1H and 1I). These data suggest that after the Golgi, SARS-CoV-2 E can engage with pathways linking the biosynthetic and endocytic routes.

Lysosome localised Envelope contributes to pH neutralisation in these organelles

To question how this minor pool of E reached lysosomes, we disrupted internalisation using a dominant-negative version of the key endocytic GTPase, Dynamin[22]. Whilst this prevented transferrin internalisation, it had no impact on the

delivery of E-Em[Site3] to lysosomes (Figure 4A – 4C). Although we cannot discount dynamin-independent internalisation, these data suggest that E is trafficked directly to lysosomes independently of the PM. Whilst b-coronaviruses assemble by budding into the ERGIC lumen, they are trafficked directly to lysosomes for secretion by lysosomal exocytosis[13]. Importantly, during infection, these secretory lysosomes are deacidified, which may limit proteolytic destruction of egressing viruses[13]. SARS-CoV-2 E is predicted to form a pentameric cation channel[23] and given the predicted parallels between the route toward lysosomes taken by both assembled virions and SARS-CoV-2 E, we wondered whether SARS-CoV-2 E contributed to pH neutralisation in lysosomes. To function as a cation channel, SARS-CoV-2 E must oligomerise. We used Fluorescence Lifetime Imaging-Forster Radius Energy Transfer (FLIM-FRET) in cells expressing both Em[Site3]- and HT [Site3]-versions of SARS-CoV-2 E to assess its oligomeric status. In this assay, protein-protein interactions are revealed as a reduction in the donor fluorophore's fluorescence lifetime. We discovered that when combined with JF646-labelled E-HT[Site3], the lifetime of E-Em[Site3] in lysosomes was reduced, suggesting that this pool of E is oligomeric (Figure 4D and 4E). E-Em[Site3]'s lifetime reduction in the Golgi was less influenced by the presence of JF646-labelled E-HT[Site3] (Figure 4D and 4E). We also used ΔDLLV versions of E and discovered that when restricted to the ER, the lifetime of E-Em[Site3] ΔDLLV was not influenced by the presence of JF646-labelled E-HT[Site3] ΔDLLV (Figure 4F and 4G). These data suggest that a progressive increase in the oligomeric status of E as it moves through the secretory pathway. We next employed a recently described reporter of lysosomal pH based upon a modified version of LAMP1 fused to luminal pH-sensitive superfolder-GFP and cytosolic pH-insensitive mCherry[24] (Figure 4 Supplement 1). Here, we discovered that pHLARE-positive lysosomes containing higher levels of E-HT[Site3] were less acidic than pHLARE-positive lysosomes in the same cell containing lower levels of E-HT[Site3] (Figure 4H-I). These data suggest that SARS-CoV-2 E is trafficked from Golgi to lysosomes and can both oligomerise and contribute to pH neutralisation in these organelles.

Discussion

Here, we developed a labelling strategy to allow visualisation of SARS-CoV-2 E. Importantly, we found that canonical tagging mechanisms are incompatible with preservation of E's biology resulting in their restriction to the ER. For C-terminal tags, we suggest that this is likely due the occlusion of a C-terminal DLLV sequence that acts as an ER-export signal. This may influence the interpretation of previously described localisations[25], vicinal[26–28] or physical[29] interactomes reported for SARS-CoV-2 E. This DLLV sequence has been described previously to function as a PDZ-ligand, and consistent with this, we observed a significant enrichment of PDZ-domain containing proteins in our vicinal proteomes from internally TurboID versions of E. We were surprised too at the degeneracy of this C-terminal sequence. Common with many secretory cargos, a C-terminal hydrophobic residue provided the majority, although not all, of the ER-export activity. This is consistent with previously described roles for these sequences in binding to COP-II components[30,31], but suggests that the context of the hydrophobic residue is important for export. Additionally, a variety of C-terminal PDZ-ligands of different classes and sequences could license at least limited export, albeit none approaching that of wildtype E, or that obtained when using versions of E bearing chimeric C-termini from MHV or MERS.

The importance of this C-terminal sequence has been demonstrated in the context of SARS-CoV infection, whereby mutation or deletion of this sequence generated revertants or reacquisition of these sequences by alternate proteins after serial passage in culture or infection in mice[32] suggesting that this sequence acts to enhance pathogenesis of coronaviral infection[21]. Recombinant versions of SARS-CoV ΔE replicated with 2- to 3-log lower titres than wildtype virus in animal models[33], but the mechanism by which E contributes to productive infection is unknown. Using a VLP system with SARS-CoV-2 proteins, we found that N packaging was reduced in VLPs generated in the absence of E, or in VLPs generated with versions of E that were restricted to the ER. These data suggest that E plays an important role in particle assembly, not necessarily by sculpting the virion, but by allowing the incorporation of N, and thus genomic RNA into the assembling particle. It may be that this defect underlies the crippled replication dynamics of recombinant ΔE

coronaviruses, or explains their aberrant morphologies[8]. Previous work using SARS-CoV proteins has demonstrated that N is packaged into VLPs in an E-dependent manner, but only in a minimal system in which N-M interactions had been disrupted[11]. Similarly, requirements for E's C-terminal hydrophobic residue in releasing extracellular nucleocapsid were exposed in an E-only system but were not observed when M was present[11]. As such, we suggest there exist differences between N packaging mechanisms between SARS-CoV and SARS-CoV-2, with E playing a more important role in this process for SARS-CoV-2. Alternatively, it is possible that the presence of S, which was absent from the minimal systems described in[11], renders N packaging more reliant upon E.

Although E is thought to contribute to the virus assembly process, coronavirus particles contain only limited amounts of this protein and the majority of E remains in the host cell[6]. We discovered that beyond the Golgi, a minor pool of E was delivered to lysosomes in a Dynamin-independent manner, suggesting that it is trafficked internally to these organelles. Coronaviral E proteins oligomerise into pentameric cation channels[5,23]. We used FLIM-FRET using our internally tagged versions of E to explore at what stage of the secretory pathway oligomerisation was observed. Whilst we could detect FRET between labelled versions of E in lysosomes, we could not detect this FRET between the same proteins when they were localised to the ER. Limited FRET was detected in the Golgi, indicating that a mixed population of oligomers was observed here and suggesting that channel formation occurs late along E's secretory journey. Using a newly developed ratiometric sensor of lysosomal pH, we discovered that E's presence resulted in lysosomal pH neutralisation, suggesting that an assembly-independent role of E is to compromise the degradative environment in these organelles, which may be important for preserving virus shed through secretory lysosomes.

Acknowledgements

Experimental Procedures

Cell Culture

STR-profiled, mycoplasma-free vials of 293T and VeroE6 cells were obtained from the Crick Cell Services Science Technology Platform. Cells were cultured in DMEM containing 10% FBS, Penicillin (100 U/mL) and Streptomycin (0.1 mg/mL).

Plasmids

Native sequences corresponding to the alpha-variant of SARS-CoV-2 Spike, Nucleocapsid and E cDNAs were purchased from GenScript Biotech: pUC57-2019-NCov-S MC_0101080; pUC57-2019-nCov-N MC_0101085; pUC57-2019-nCOV E MC_0101078. Codon-optimised Spike and Nucleocapsid sequences were kind gifts from Prof. Neil McDonald (Crick) and were cloned similarly into pCR3.1. A sequence corresponding to the native sequence of Membrane was synthesised by GeneWIZ. Coding sequences were amplified by PCR and inserted *EcoRI-NotI* into pCR3.1 for mammalian expression. An internal *EcoRI* site in E was removed by silent mutagenesis. Insertion of HaloTag in the E coding sequence was performed using HiFi DNA Assembly, with HaloTag amplified by PCR from pHTN-HaloTag CMV-neo (Promega), with a Gly-Gly-Gly-Ser linker placed either side of the HaloTag at site 3

and 4, a single linker placed between E N/C-terminus and HaloTag at tag sites 1 or 5, and a Gly-Gly-Gly-Ser-HaloTag-Gly-Gly-Gly-Ser-Glu-Glu inserted at site 2. Hemagglutinin (HA)-TurboID tagging at sites 3 and 4 was performed by HiFi DNA Assembly, with HA-TurboID amplified by PCR from 3xHA-TurboID-NLS_pCDNA3 (Addgene #107171) and inserted with a Gly-Gly-Gly-Ser linker either side of the HA-TurboID sequence. Emerald-TurboID was used for a cytosolic control in proximity biotinylation experiments and was generated by using HiFi DNA Assembly to assemble Emerald-TurboID in a pLXIN vector. mEmerald was amplified from mEmerald-Sec61b-C1 (Addgene #90992) and TurboID amplified from 3xHA-TurboID-NLS_pCDNA3, with *AgeI* and *EcoRI* restriction sites for insertion into pEGFP-C1. pHLARE plasmids were a kind gift from Prof. Diana Barber (University of California, San Francisco). HA-Dynamin2 K44A was a kind gift from Prof. Stuart Neil (King's College London).

Antibodies and fluorescent labels

An antibody against GAPDH (MAB374) was from Millipore; an antibody against SARS-CoV-2 Spike (GTX632604) was from GeneTex; an antibody against SARS-CoV-2 Nucleocapsid (BS-41408R) was from Bioss; an antibody against SARS-CoV Membrane (101-401-A55) was from (Rockland); an antibody against ERGIC53 (E1031) was from Sigma-Aldrich; an antibody against GM130 (610822) was from BD Biosceinces; an antibody against TGN46 (ab50595) was from Abcam; an antibody against EEA1 (610457) was from BD Biosciences; an antibody against O-GlcNAc (CTD110.6) was from Sigma; an antibody against HA.11 (16B12) was from Biolegend; an antibody against HaloTag (G9211) was from Promega; an antibody against GFP (7.1/13.1) was from Roche; an antibody against RER1 (HPA051400) was from Sigma-Aldrich; an antibody against PALS1 (17710-1-AP) was from Proteintech; an antibody against GORAPS2 (10598-1-AP) was from Proteintech; an HRP-conjugated antibody against Streptavidin (S911) was from Invitrogen; Alexa conjugated secondary antibodies were from Invitrogen and HRP-conjugated secondary antibodies were from Millipore. IRDye 800 CW (925-32210) and IRDye 680 RD (925-68071) were from LI-COR Biosciences. Alexa-647 conjugated Transferrin was from Molecular Probes. Janelia Fluor 646 HaloTag ligand (GA1120),

Oregon Green Halotag ligand (G2801), and Tetramethylrhodamine HaloTag ligand (G8251) were from Promega.

Transient transfection of cDNA

VeroE6 cells were transfected using Lipofectamine-3000 (Life Technologies) according to the manufacturer's instructions. 293T cells were transfected using linear 25-kDa polyethylenimine (PEI, Polysciences, Inc.), as described previously[34].

Fixed cell imaging

VeroE6 cells were plated at 40,000 per well on 13mm No. 1.5 coverslips and transfected as described the following day. If cells were transfected with HaloTag-versions of SARS-CoV-2 E, cells were treated with 1 µM Oregon Green Halo ligand for 20 minutes and then washed 3 times with complete media, with a 5–10-minute incubation on the final wash. All cells were washed once with PBS before being fixed using 4 % paraformaldehyde for 20 minutes. Cells that required immunolabelling were permeabilised with 0.1 % Triton-X100 in PBS, washed 3 times in PBS, and blocked in 5% FBS for 1 hour. After primary and secondary antibody incubations, coverslips were mounted on X50 SuperFrost microscope slides using Mowiol. Imaging was performed either using a Zeiss LSM 880 (as previously described) or a Nikon Eclipse Ti2 microscope fitted with a confocal Andor Spinning Disk and Zyla 5.5 sCMOS camera. To limit overexpression, cells were fixed 16-18 hours post transfection. E phenotype quantification was performed on 50 cells per condition, with sample identification randomised and blinded during scoring.

Live cell imaging

Cells stably expressing the indicated proteins, or edited to express fluorescent proteins, were plated in 4- or 8-chamberslides (Ibidi). VeroE6 cells were plated at 40,000 per well in µ-slide ibiTreat 4 well Ibidi chambers and transfected as described the following day. After 16-18hrs, cells were treated with 200nM JF646 Halo-ligand in complete media for 20mins and were then washed twice in growth media before

being imaged in FluoroBright DMEM supplemented with 10% FBS, 4mM L-glutamine, Penicillin (100 U/mL) and Streptomycin (0.1 mg/mL). Airyscan imaging was performed using a Zeiss LSM 880 inverted microscope with a Plan Apo 63X/1.4NA objective fitted with a Fast Live Cell Airyscan detector, definite focus, and heat and CO_2 incubation. Acquired images were processed using Zeiss' "Auto" 2D Airyscan processing, and image brightness levels and image crops were adjusted and performed using the FIJI distribution of ImageJ. To limit overexpression, cells were imaged between 16-18 hours post transfection.

FLIM-FRET Imaging

VeroE6 cells were transfected as previously described with SARS-CoV-2 E-Em^{Site3} or E-Em^{Site3} ΔDLLV mutant as the fluorescence donor, and either empty vector for a single colour control or Halo tagged SARS-CoV-2 E WT or ΔDLLV mutant illuminated with Tetramethylrhodamine (TMR) HaloTag ligand for the fluorescence acceptor. A 1:3 ratio was used for fluorescence donor to acceptor. TMR HaloTag ligand was applied to cells for 30minutes before the cells were washed thrice in growth media and then incubated for 30minutes before cells were imaged in live cell imaging media. FLIM imaging was performed on a Leica TCS SP8 Multiphoton FALCON with a HC PL APO CS2 63x/1.40 oil objective using 470nm and 552nm laser lines at 100Hz scan speed scanning by line, with samples incubated at 37°C and in 5% CO_2. Time-correlated single photon counting fluorescence lifetime data was acquired using a PicoQuant PDL 800-D unit. Raw files were then exported into FLIMfit software[35] for analysis. Intensity images for each FLIM image were exported into FIJI and a custom script was written to segment each lysosome allowing the fluorescence lifetime of each lysosome to be calculated individually in FLIMfit. The Golgi was excluded from this analysis and segmented separately, with one fluorescence lifetime calculated across the entire Golgi from each cell. For analysis of the endoplasmic reticulum lifetime in SARS-CoV-2 E ΔDLLV cells, the whole area of the cell was used to calculate the fluorescence lifetime. For all FLIM analysis, no binning was used, and a single exponential curve was fitted to the data to calculate fluorescence lifetime on a pixel-wise basis.

Transferrin Internalisation Assay

VeroE6 cells plated on coverslips were transfected with equivalent amounts of mEmerald tagged SARS-CoV-2 E and either empty plasmid or dominant-negative HA tagged Dynamin2 K44A. After 16hrs, cells were treated with Transferrin-647 (T23366) purchased from ThermoFisher at 10µg/ml resuspended in growth media for 2 minutes before being washed once in ice-cold PBS and fixed immediately in 4%PFA. Untreated cells ("0 minutes") were fixed without being treated with Transferrin-647. Cells were then prepared for fixed cell imaging, with the presence of HA tagged Dynamin2-K44A detected by detection by an HA antibody. The number of transferrin and SARS-CoV-2 E puncta was analysed in FIJI using a custom written script to isolate the lysosomal puncta, with these counts corrected for differing cell area.

pHLARE Assay

VeroE6 cells were transfected with Halo tagged SARS-CoV-2 E and pHLARE plasmids at equal amounts, and after 16 hours cells were incubated with JF646 Halo ligand and imaged by live-cell microscopy on a Zeiss LSM 880 inverted microscope with a Plan Apo 63X/1.4NA objective in green, red and far-red channels scanning by line. Images were analysed in FIJI using a custom written script that removed background from all channels, identified lysosomes by their presence in the mCherry red channel, classified these as either E-high or E-low/absent, and then measured the Integrated Density (IntDen) in the 488 channel and the 561 channels. E-high/low lysosomes were determined by eye and equated to at least a 10-fold difference between the mean of the mean grey intensities of the E-high and E-low lysosomes. The ratios between the 488 and 561 channels for E-high and E-low/absent for each lysosome were then averaged across the cell and averaged across the total number of cells recorded. For positive controls, VeroE6 cells were transfected with pHLARE plasmids alone and then after 16hrs were treated with either 200nM BafilomycinA1 (19-148) from Sigma-Aldrich for 150 minutes, 10µM Chloroquine diphosphate (C6628) from Sigma-Aldrich for 160 minutes, 10mM Ammonium Chloride (254134) from Sigma-Aldrich for 180 minutes, or were untreated, and imaged in green and red channels using the system described. Images were analysed in FIJI using a custom-written script that removed background in all channels and then identified the

lysosomes by their presence in the mCherry red channel, and then measured the Integrated Density of each of these lysosomes in both green and red channels. Data was collated as described above for SARS-CoV-2 E experiments.

TurboID Proximity Biotinylation, Pull Down, and Mass Spectrometry

HEK293T cells were grown for at least 5 days in biotin-free growth media to remove all sources of biotin. These were then transferred to T75 flasks, with 3 flasks seeded per condition. Cells were transfected with either WT or mutant E-HA-TurboID or E-TurboID (cytosolic control) constructs using PEI, with 1800uL optiMEM, 36ug DNA, and 72uL PEI used per flask. After 18hrs exactly, cells were biotinylated by incubation for 20minutes in biotin-free growth media supplement with 50µM biotin (Sigma-Aldrich). At 20minutes exactly, flasks were placed on ice and washed 1x with ice-cold PBS to halt the biotinylation reaction. Cells were then scrapped in 10ml of ice-cold PBS and pelleted, with pellets kept on ice until all samples had been prepared. Cell pellets were then lysed by 30min incubation at 4°C in 1ml RIPA buffer (150mM NaCl, 50mM Tris-HCl pH8, 1% NP40, 0.5% Sodium deoxycholate, 0.4% SDS, 1mM EDTA) supplemented with cOmplete EDTA-free protease inhibitors (Roche) and 167U/ml of Benzonase Nuclease (Sigma-Aldrich). During this time pre-acetylated NeutrAvidin agarose beads (Pierce) were washed 4 times with 10x their volume in lysis buffer, with 40µL beads used per sample. NeutrAvidin bead acetylation was necessary to stop the Neutravidin being cleaved from the agarose beads during on-bead digestion and performed prior to the day of pulldown by two 30min incubations of beads with 10mM Sulfo-NHS acetate (ThermoFisher) on a rotating wheel followed by quenching in 90mM Tris-HCl pH7.5. Lysed cell pellets were centrifuged at 14,000rpm at 4°C for 15mins to sediment undigested nuclear debris, and lysate supernatants were mixed with equal amounts of washed acetylated NeutrAvidin beads and rotated at room temperature for 2hrs. The beads were then washed 3xs in 500uL RIPA buffer and 6xs in 25mM HEPES pH8.5, with the beads rotated for 3mins at room temperature for each wash. After the final wash, beads were resuspended in 100uL 25mM HEPES pH8.5 and 100ng of Lysyl endopeptidase LysC (WAKO) was added to each sample, with this mixture incubated for 16hrs at 37°C in a hooded ThermoMixer at 1,200rpm. Each bead supernatant was then transferred to a new Eppendorf and mixed with 100ng Trypsin

(Pierce) and incubated at 37°C for 6hrs. The solutions were then acidified to a final concentration of 0.5% trifluoroacetic acid (TFA). Digested samples were loaded onto Evotips (according to manufacturer's instructions) and washed once with aqueous acidic buffer (0.1% formic acid in water) before loading onto an Evosep One system coupled to an Orbitrap Fusion Lumos (ThermoFisher Scientific). The Evosep One was fitted with a 15cm column (PepSep) and a predefined gradient for a 44minute method was employed. The Orbitrap Lumos was operated in data-dependent mode (1 second cycle time), acquiring IT HCD MS/MS scans in rapid mode after an OT MS1 survey scan (R=60,000). The MS1 target was 4E5 ions whereas the MS2 target was 1E4 ions. The maximum ion injection time utilized for MS2 scans was 300 ms, the HCD normalized collision energy was set at 32 and the dynamic exclusion was set at 15 seconds. Acquired raw files were processed with MaxQuant v1.5.2.8[36]. Peptides were identified from the MS/MS spectra searched against Homo sapiens and SARS-CoV-2 proteomes (UniProt) as well as Gallus gallus Avidin (UniProt) and sequences of all TurboID-tagged constructs using Andromeda[37] search engine. Methionine oxidation, Acetyl (N-term), Acetyl (K) and Deamidation (NQ) were selected as variable modifications. The enzyme specificity was set to Trypsin with a maximum of 2 missed cleavages. The precursor mass tolerance was set to 20 ppm for the first search (used for mass re-calibration) and to 4.5 ppm for the main search. The datasets were filtered on posterior error probability (PEP) to achieve a 1% false discovery rate on protein, peptide and site level. Other parameters were used as pre-set in the software. 'Unique and razor peptides' mode was selected to allow identification and quantification of proteins in groups (razor peptides are uniquely assigned to protein groups and not to individual proteins). Intensity based absolute quantification (iBAQ) in MaxQuant was performed using a built-in quantification algorithm[36] enabling the 'Match between runs' option (time window 0.7 minutes) within replicates. MaxQuant output files were processed with Perseus, v1.4.0.2[38]. Data were filtered to remove contaminants, protein IDs originating from reverse decoy sequences and only identified by site. iBAQ intensities were log2 transformed, normalized by median subtraction, and filtered for the presence of 15 valid values. Missing values were imputed from normal distributions. P-values were calculated by two-sample t-tests using Benjamini—Hochberg FDR correction for multiple testing. Crapome data was obtained from Crapome V2[39].

Immunoprecipitation Assay

25 million 293T cells in a 150 mm dish were transfected with 40 mg pCR3.1 E-HT[Site3] or pCR3.1 using Polyethyleneimine. After 48 hours, cells were rinsed briefly in ice cold PBS, were lifted from the dish using a cell scraper, collected by centrifugation at 300 x g and lysed on ice in 1 mL of HNE buffer (50 mM Hepes, pH 7.5, 150 mM NaCl, 1 mM EDTA, 1% glycerol) supplemented with 0.5 % Digitonin, protease inhibitors (Complete mini) and phosphatase inhibitors (PhosStop). Lysis was performed in low-bind microfuge tubes (Eppendorf). Insoluble material was removed by centrifugation at 14,000 x g for 2 minutes and the supernatant was incubated with 50 ml HNG-washed agarose beads (Chromotek) with end-over-end rotation for 15 minutes to capture non-specific binding proteins. Beads were collected by centrifugation and discarded. The supernatant was incubated with 50 ml HNG-washed HaloTrap-agarose beads (Chromotek) with end-over-end rotation for 15 minutes to capture specific binding proteins. Beads were washed thrice in HNG buffer and were transferred to fresh tubes. Bead-bound proteins were released by boiling in 2 x LDS sample buffer. For analysis of post-translational modification on E, 600,000 293T cells in a 35 mm dish were transfected with 2 mg pCR3.1 E-HT[Site3], or derivatives. After 16 hours, cells were lysed in 1 mL TNE buffer (50 mM Tris.HCl, pH 7.5, 150 mM NaCl, 1 mM EDTA, 1% glycerol) supplemented with 1 % NP40 substitute, protease and phosphatase inhibitors. Insoluble material was removed by centrifugation at 14,000 x g for 2 minutes and the supernatant was incubated with 10 ml TNG-washed agarose beads (Chromotek) with end-over-end rotation for 15 minutes to capture non-specific binding proteins.

Virus Like Particle Production Assay

7.5 million 293T cells in a 100 mm dish were transfected with a mixture comprising 5 mg pCR3.1 SARS-CoV-2 S (codon optimised), 3 mg pCR3.1 SARS-CoV-2 M, 3 mg pCR3.1 SARS-CoV-2 E (or derivatives) and 1 mg of pCR3.1 SARS-CoV-2 N (codon optimised). Codon optimised sequences were chosen to reduce chances of

contamination of the Crick in-house testing pipeline. Media was changed after 6 hours. 48 hours after transfection, supernatants were clarified by centrifugation (300 x g, 2 minutes) and passed through a 0.45 mm syringe filter. Supernatants were underlaid with a PBS 20% sucrose cushion and subject to ultracentrifugation in a Beckman SW41 Ti swinging bucket rotor at 28,000 rpm for 3 hours at 4 ^{o}C. Supernatants were removed and pellets were resuspended in 30 mL PBS and incubated overnight at 4 ^{o}C. The next morning, 30 mL of 2 x LDS-sample buffer was added for sample recovery. Cellular fractions were obtained by lifting cells with PBS and collecting them by centrifugation (300 x g, 2 minutes) before resuspending the pellet in fresh PBS and adding an equal volume of 2 x LDS sample buffer.

Sequence Alignments

Alignment of SARS-CoV E and SARS-CoV-2 E was performed using T-Coffee[40]. Aligned sequences were then exported and viewed in Jalview[41], and residues colour coded using ClustalX colour map.

Gene Ontology Analysis

Gene ontology cellular compartment (GO:CC) data was used to categorise the subcellular distribution of proteins identified from proteomic analysis. The GO:CC terms used were ER: GO:0005783, ERGIC: GO:0005793, Golgi: GO:0005794, Lysosomal: GO:0005768 (endosome), GO:0005764 (lysosome).

Statistical analysis

2-tailed Student's T-tests, or ordinary 1-way ANOVA with the indicated post-hoc tests were used to assess significance between test samples and controls and were performed using GraphPad Prism. N-numbers given as the number of independent experiments, n-numbers given as the number of cells analysed.

Figure Legends

Figure 1: Export of SARS-CoV-2 Envelope from the ER to the Golgi is regulated by a C-terminal PDZ-ligand.

A. Sequence of SARS-CoV and SARS-CoV-2 E, and SARS-CoV-2 EΔDLLV. Transmembrane domain, C-terminal PDZ ligand and position of tagging sites indicated. Amino acids coloured according to physiochemical properties. **B.** VeroE6 cells were transfected with plasmids encoding the indicated SARS-CoV-2 E-HT^{Site3} plasmids and illuminated with Janelia Fluor (JF) 646. **C**. Quantification of the localisation of the differently tagged JF646-illuminatd HaloTag versions of SARS-CoV-2 E-HT^{Site3} from B. For each condition, 50 cells were imaged and the extent of localisation in each of 4 categories (ER, Golgi, vesicles, or plasma membrane) was scored. **D**. VeroE6 cells were transfected with plasmids encoding the indicated SARS-CoV-2 E-HT^{Site3} plasmids, illuminated with Oregon Green, fixed, and stained with the indicated antisera. A plasmid encoding LAMP1-tdTomato was co-expressed to illuminate lysosomes. **E, F**. VeroE6 cells were transfected with plasmids encoding the indicated SARS-CoV-2 E-HT^{Site3} plasmids and illuminated with JF646. Quantification of localisation from 50 imaged cells provided in F. **G**. Schematic of the rescue strategy of indicated SARS-CoV-2 E-HT^{Site5}. **H, I**. VeroE6 cells were transfected with plasmids encoding the indicated SARS-CoV-2 E-HT^{Site5} plasmids and illuminated with JF646. Quantification of localisation from 50 imaged cells provided in I.

Figure 1 Supplement 1: Validation of visualisation strategy using mEmerald labelled versions of SARS-CoV-2 Envelope and sequence requirements for ER export of SARS-CoV-2 Envelope

A, B. VeroE6 cells were transfected with plasmids encoding the indicated SARS-CoV-2 E-Em^{Site3} plasmids. Quantification of localisation from 50 imaged cells provided in B with comparator of HT versions of E from Figure 1C provided. **C.** Sequence of C-terminal deletions of SARS-CoV-2 E. **D, E**. VeroE6 cells were transfected with plasmids encoding the indicated C-terminal deletions or mutations of SARS-CoV-2 E-Em^{Site3}. Quantification of localisation from 50 imaged cells provided in E. **F.** Sequence of PDZ-ligand switched versions of mEmerald tagged SARS-CoV-

2 E or chimeric versions of SARS-CoV-2 E in which the C-terminal PDZ-ligand was exchanged for the corresponding sequence from Murine Hepatitis Virus (MHV) Strain-S or Middle East Respiratory Syndrome (MERS) Virus. **G, H.** VeroE6 cells were transfected with plasmids encoding the indicated PDZ-ligand switched versions of SARS-CoV-2 E-Em^{Site3} or chimeric versions of SARS-CoV-2 E described in D. Quantification of localisation from 50 imaged cells provided in F. The class of PDZ ligand is indicated, with Class I defined by -X-[S/T]-X-ɸ, Class II defined by -X- ɸ-X-ɸ, Class III defined by -X-[D/E/K/R]-X- ɸ[42]. **I, J.** VeroE6 cells were transfected with plasmids encoding SARS-CoV-2 E-Em^{Site3}, or SARS-CoV-2 E-Em^{Site3} P71L (beta-variant of SARS-CoV-2 E). Quantification of localisation from 50 imaged cells provided in J.

Figure 1 Supplement 2: Identification of O-GlcNAcylation sites on SARS-CoV-2 Envelope and the dependence of O-GlcNAcylation on ER localisation

A, B. 293T cells expressing the indicated versions of SARS-CoV-2 E-HT^{Site3} were immunoprecipitated with HaloTrap agarose beads. Cell lysates and captured fractions were examined by western blotting with anti-HaloTag or anti-O-GlcNAc CTD110.6 antisera. Western blots indicative of N = 3 independent experiments. **C.** Quantification of the O-GlcNAcylation upon SARS-CoV-2 E-HT^{Site3} variants (Mean ± S.D. from N = 3 independent experiments, significance calculated with a 1-way ANOVA with Dunnett's multiple comparisons test. All non-indicated values were non-significant, although for SARS-CoV-2 E-HT^{Site3} S68A, P = 0.054.

Figure 2: The Golgi localisation of SARS-CoV-2 Envelope supports packaging of Nucleocapsid into Virus Like Particles (VLPs)

A. 293T cells were transfected with plasmids encoding SARS-CoV-2 N, S, M and either empty vector, E or EΔDLLV. VLP and cellular fractions were resolved and examined by western blotting with the indicated antisera. Nucleocapsid in the VLP fraction was quantified, Mean ± S.D. presented from N = 3 independent experiments. P = <0.0001, as determined by 1-way ANOVA.

Figure 3: A strategy to illuminate the vicinal proteome of SARS-CoV-2 Envelope.

A. Volcano plot depicting peptides recovered from a neutravidin immunoprecipitation from 293T cells expressing HA-TurboID SARS-CoV-2 E or HA-TurboID and subject to a 20-minute biotinylation. N = 3. **B**. HEK293T cells were transfected with Halo tagged SARS-CoV-2 E and subjected to a Halo-Trap immunoprecipitation and examined by western blotting with the indicated antisera (N = 3).

Figure 3 Supplement 1: A strategy to illuminate the vicinal proteome of SARS-CoV-2 Envelope.

A. VeroE6 cells were transfected with plasmids encoding HA-TurboID versions of SARS-CoV-2 E, fixed, and stained with anti-HA antisera. **B.** Hierarchical clustering performed on the median adjusted IBAQ values of each proteomic sample calculated and plotted by average Euclidean distance. **C.** Principle component analysis (PCA) on median averaged data across the three repeats for each sample. Red dots/text indicates WT-like SARS-CoV-2 E, green indicates ΔDLLV-like SARS-CoV-2 E, and grey indicates the cytoplasmic control. **D.** Volcano plot depicting peptides recovered from a neutravidin immunoprecipitation from 293T cells expressing either SARS-CoV-2 E-HA-TurboID or SARS-CoV-2 E-HA-TurboID ΔDLLV, and subject to a 20-minute biotinylation. N = 3. All PDZ domain containing proteins identified are highlighted. **E, F, G, H.** Volcano plots depicting peptides recovered from a neutravidin immunoprecipitation from 293T cells expressing either SARS-CoV-2 E-HA-TurboID or SARS-CoV-2 E-HA-TurboID ΔDLLV, and subject to a 20-minute biotinylation. N = 3. Gene Ontology was used to assign recovered proteins to subcellular localisations. Percentages were counted from proteins that changed abundance by more than 2-fold and were statistically significant at P < 0.05. **I.** Volcano plot depicting peptides recovered from a neutravidin immunoprecipitation from 293T cells expressing either HA-TurboID SARS-CoV-2 E-HA-TurboID or unconjugated HA-TurboID, and subject to a 20-minute biotinylation. N = 3. All

adaptor proteins (AP) identified are highlighted, with colours corresponding to the different AP complexes.

Figure 4: Lysosomal SARS-CoV-2 Envelope is oligomeric and can de-acidify lysosomes

A. VeroE6 cells were transfected with plasmids encoding SARS-CoV-2 E-Em^{Site3} and either empty vector or a plasmid encoding HA-tagged Dynamin2 K44A. Cells were incubated with Alexa647-labelled Transferrin for 2 minutes and then fixed, stained with antisera against HA, and imaged. **B**. Quantification of cells from A demonstrating that expression of HA-Dynamin2 K44A prevents internalisation of Alexa647-labelled transferrin. Mean ± S.D. displayed, P <0.0001, by 2-tailed T-Test with 25 imaged cells. **C.** Quantification of SARS-CoV-2 E-Em^{Site3} puncta revealed that Dynamin2 K44A had no bearing on the number of E-Em^{Site3} puncta, either in the presence or absence or Alexa-647 labelled transferrin. Mean ± S.D. displayed, P = 0.27, as determined by 2-tailed T-Test with 25 imaged cells per condition. **D**. VeroE6 cells were transfected with E-Em^{Site3} and E-HT^{Site3} versions of SARS-CoV-2 E at a ratio of 1:3. HaloTag versions of SARS-CoV-2 E were illuminated with HaloTag Tetramethyl Rhodamine (TMR) ligand. Cells were examined by confocal and FLIM-FRET imaging and a rainbow LUT was used to display mEmerald lifetime. **E**. The mEmerald signal was segmented into lysosomal or Golgi classes and the lifetime of mEmerald in the presence or absence of HaloTag was calculated in each class. Mean ± S.D. displayed, lysosomal P = <0.0001, Golgi P = 0.02, as determined by 2-tailed T-Test from 15 imaged cells per condition. **F**. VeroE6 cells were transfected with E-Em^{Site3} and E-HT^{Site3} versions of SARS-CoV-2 EΔDLLV at a ratio of 1:3. HaloTag versions of SARS-CoV-2 E were illuminated with HaloTag Tetramethyl Rhodamine (TMR) ligand and a rainbow LUT was used to display mEmerald lifetime. Cells were examined by confocal and FLIM-FRET imaging. **G.** The mEmerald signal localised to the ER and the lifetime of mEmerald in the presence or absence of HaloTag TMR was calculated. Mean ± S.D. displayed, P = 0.09, as determined by 2-tailed T-Test from 15 imaged cells per condition. **H**. Example image of VeroE6 cells

expressing both pHLARE reporter and SARS-CoV-2 E-HT^{Site3} illuminated with JF646. Examples of E-HT^{Site3}-low and E-HT^{Site3}-high lysosomes are displayed. **I.** VeroE6 cells were transfected with SARS-CoV-2 E-HT^{Site3} and the pHLARE reporter. JF646 was used to illuminate the HaloTag. Ratiometric imaging of GFP and mCherry signals was used to assess lysosomal pH in JF646-positive and JF646-negative lysosomes within the same cell. Mean ± S.D. displayed from n = 1364 JF646-high and n = 2761 JF646-low lysosomes from N = 28 cells. P = 0.01, as determined by paired 2-tailed T-test.

Figure 4 Supplement 1: Validation of the pHLARE assay

A. VeroE6 cells were transfected with the pHLARE reporter and treated with the indicated compounds (Bafilomycin A1, 200nM, 150 mins; Chloroquine, 10μM, 160 mins; Ammonium Chloride, 10mM, 180 mins). Cells were fixed and imaged and the ratio of sfGFP to mCherry fluorescence in mCherry positive lysosomes was calculated. Mean ± S.D. presented from N = 10 cells per condition, significance calculated with 1-way ANOVA.

Supplementary Table 1:

All data from label-free quantification of proximity biotinylation proteomics of HA-TurboID tagged SARS-CoV-2 E, SARS-CoV-2 E mutants, and HA-TurboID cytoplasmic controls.

Supplementary Table 2:

Data subset of label free quantification data of proximity biotinylation proteomics of HA-TurboID tagged SARS-CoV-2 E compared to HA-TurboID cytoplasmic control.

Supplementary Table 3:

Data subset of label free quantification data of proximity biotinylation proteomics of HA-TurboID tagged SARS-CoV-2 E compared to SARS-CoV-2 E ΔDLLV.
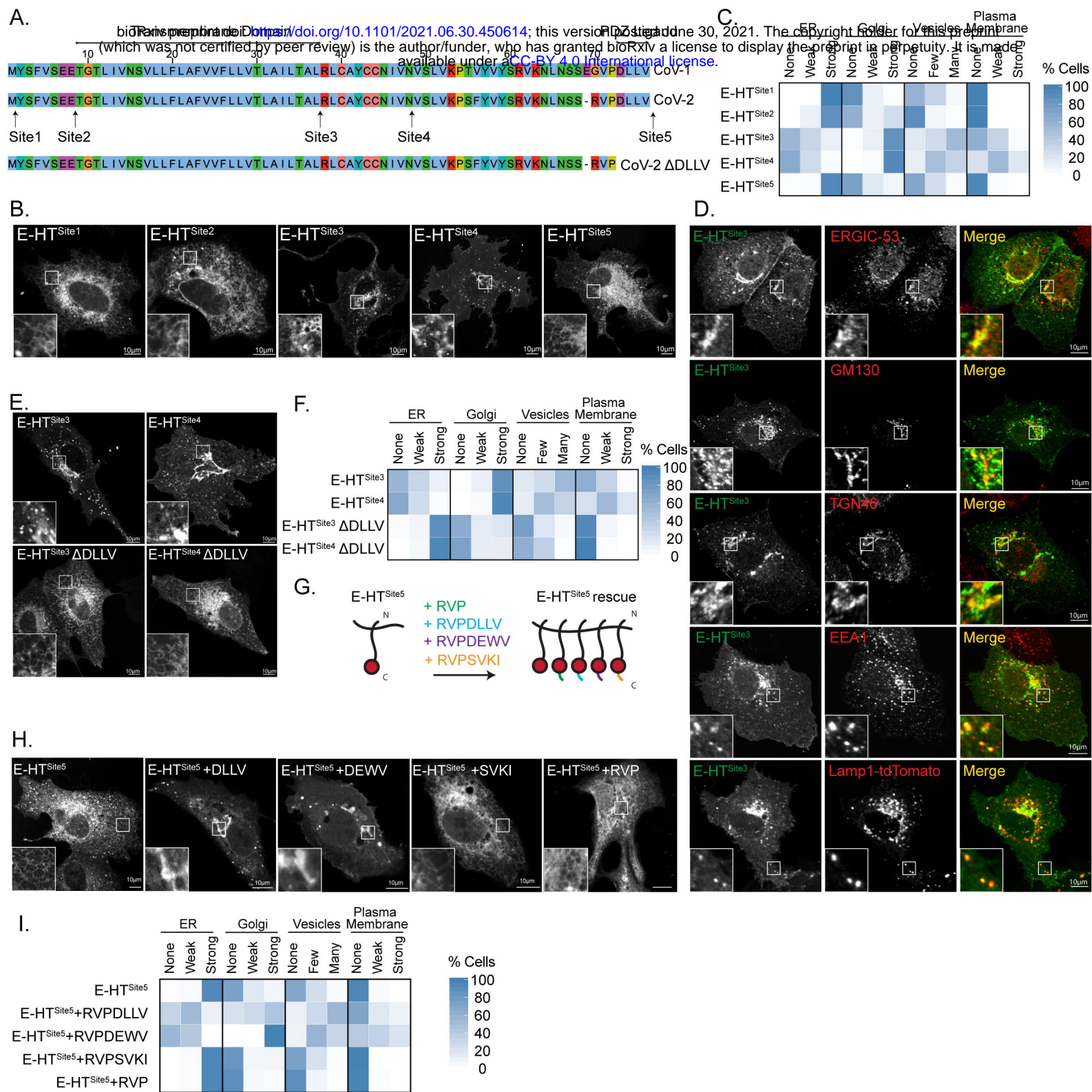
References

1.   Hu, B., Guo, H., Zhou, P. & Shi, Z. L. Characteristics of SARS-CoV-2 and COVID-19. *Nature Reviews Microbiology* **19**, 141–154 (2021).

2.   Walls, A. C. *et al.* Structure, Function, and Antigenicity of the SARS-CoV-2 Spike Glycoprotein. *Cell* **181**, 281-292.e6 (2020).

3.   Lan, J. *et al.* Structure of the SARS-CoV-2 spike receptor-binding domain bound to the ACE2 receptor. *Nature* **581**, 215–220 (2020).

4.   Mousavizadeh, L. & Ghasemi, S. Genotype and phenotype of COVID-19: Their roles in pathogenesis. *Journal of Microbiology, Immunology and Infection* **54**, 159–163 (2020).

5.   Wilson, L., Mckinlay, C., Gage, P. & Ewart, G. SARS coronavirus E protein forms cation-selective ion channels. *Virology* **330**, 322–331 (2004).

6.   Venkatagopalan, P., Daskalova, S. M., Lopez, L. A., Dolezal, K. A. & Hogue, B. G. Coronavirus envelope (E) protein remains at the site of assembly. *Virology* **478**, 75–85 (2015).

7.   Stertz, S. *et al.* The intracellular sites of early replication and budding of SARS-coronavirus. *Virology* **361**, 304–315 (2007).

8.   Schoeman, D. & Fielding, B. C. Coronavirus envelope protein: Current knowledge. *Virology Journal* **16**, 1–22 (2019).

9.   Ho, Y., Lin, P. H., Liu, C. Y. Y., Lee, S. P. & Chao, Y. C. Assembly of human severe acute respiratory syndrome coronavirus-like particles. *Biochem. Biophys. Res. Commun.* **318**, 833–838 (2004).

10.   Hsieh, P.-K. *et al.* Assembly of Severe Acute Respiratory Syndrome Coronavirus RNA Packaging Signal into Virus-Like Particles Is Nucleocapsid Dependent. *J. Virol.* **79**, 13848–13855 (2005).

11.   Tseng, Y. T., Wang, S. M., Huang, K. J. & Wang, C. T. SARS-CoV envelope protein palmitoylation or nucleocapid association is not required for promoting virus-like particle production. *J. Biomed. Sci.* **21**, 1–11 (2014).

12.   Siu, Y. L. *et al.* The M, E, and N Structural Proteins of the Severe Acute
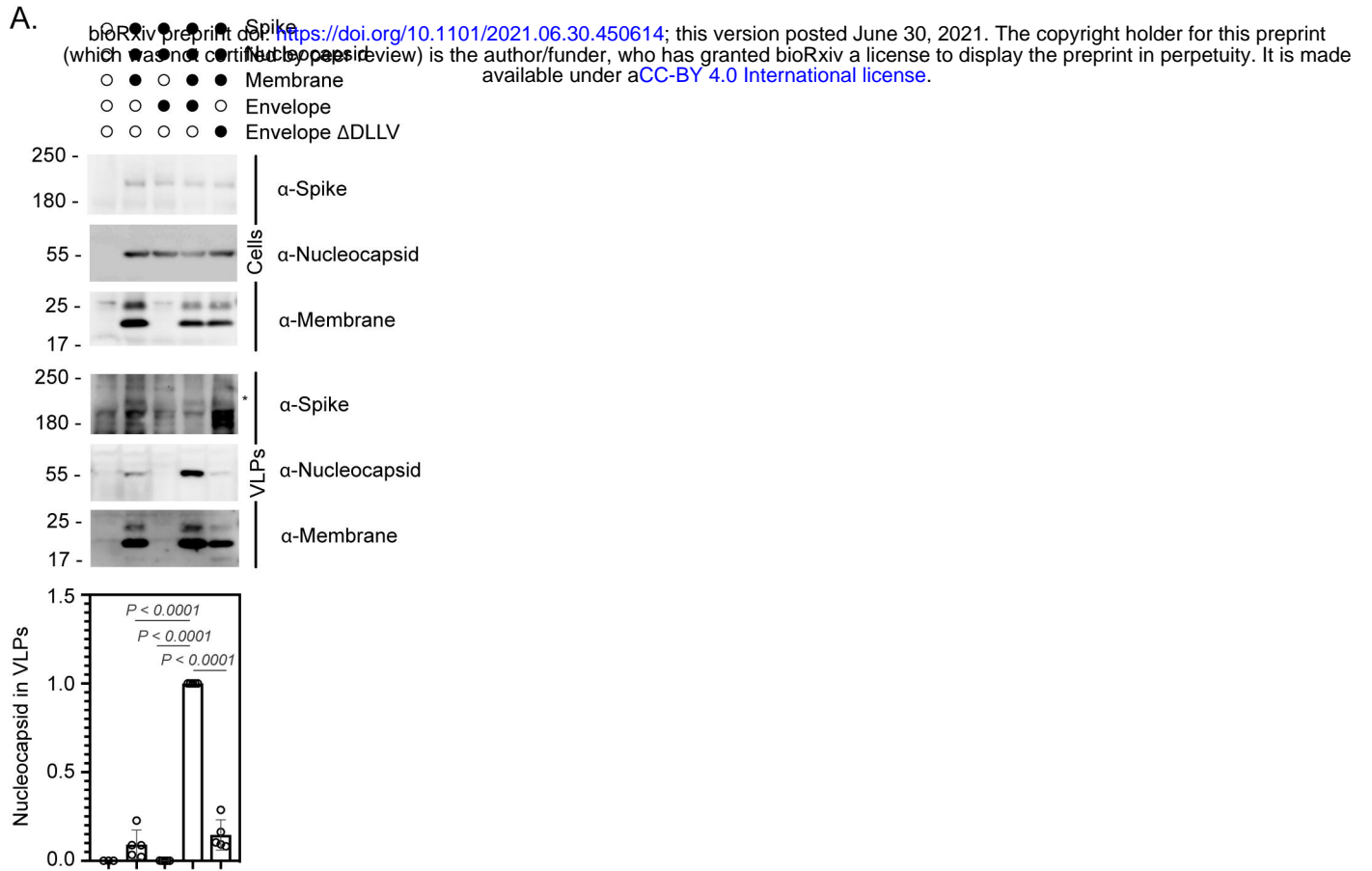
Respiratory Syndrome Coronavirus Are Required for Efficient Assembly, Trafficking, and Release of Virus-Like Particles. *J. Virol.* **82**, 11318–11330 (2008).

13. Ghosh, S. *et al.* β-Coronaviruses Use Lysosomes for Egress Instead of the Biosynthetic Secretory Pathway. *Cell* **183**, 1520-1535.e14 (2020).

14. Miao, G. *et al.* ORF3a of the COVID-19 virus SARS-CoV-2 blocks HOPS complex-mediated assembly of the SNARE complex required for autolysosome formation. *Dev. Cell* **56**, 427-442.e5 (2021).

15. Chai, J. *et al.* Structural basis for SARS-CoV-2 envelope protein recognition of human cell junction protein PALS1. *Nat. Commun.* **12**, 1–6 (2021).

16. Nieto-Torres, J. L. *et al.* Subcellular location and topology of severe acute respiratory syndrome coronavirus envelope protein. *Virology* **415**, 69–82 (2011).

17. Cohen, J. R., Lin, L. D. & Machamer, C. E. Identification of a Golgi Complex-Targeting Signal in the Cytoplasmic Tail of the Severe Acute Respiratory Syndrome Coronavirus Envelope Protein. *J. Virol.* **85**, 5794–5803 (2011).

18. Branon, T. C. *et al.* Efficient proximity labeling in living cells and organisms with TurboID. *Nat. Biotechnol.* **36**, 880–898 (2018).

19. Shepley-Mctaggart, A. *et al.* Sars-cov-2 envelope (e) protein interacts with pdz-domain-2 of host tight junction protein zo1. *PLoS One* **16**, e0251955 (2021).

20. Javorsky, A., Humbert, P. O. & Kvansakul, M. Structural basis of coronavirus E protein interactions with human PALS1 PDZ domain. *Commun. Biol.* **4**, 1–8 (2021).

21. Jimenez-Guardeño, J. M. *et al.* The PDZ-Binding Motif of Severe Acute Respiratory Syndrome Coronavirus Envelope Protein Is a Determinant of Viral Pathogenesis. *PLoS Pathog.* **10**, 1004320 (2014).

22. Antonny, B. *et al.* Membrane fission by dynamin: what we know and what we need to know. *EMBO J.* **35**, 2270–2284 (2016).

23. Mandala, V. S. *et al.* Structure and drug binding of the SARS-CoV-2 envelope

protein transmembrane domain in lipid bilayers. *Nat. Struct. Mol. Biol.* **27**, 1202–1208 (2020).

24.   Webb, B. A. *et al.* pHLARE: A new biosensor reveals decreased lysosome pH in cancer cells. *Mol. Biol. Cell* **32**, 131–142 (2021).

25.   Miserey-Lenkei, S. *et al.* A comprehensive library of fluorescent constructs of SARS-CoV-2 proteins and their initial characterisation in different cell types. *Biol. Cell* **0**, 1–18 (2021).

26.   Laurent, E. M. *et al.* Global BioID-based SARS-CoV-2 proteins proximal interactome unveils novel ties between viral polypeptides and host factors involved in multiple COVID19-associated mechanisms. *bioRxiv* 2020.08.28.272955 (2020). doi:10.1101/2020.08.28.272955

27.   St-Germain, J. R. *et al.* A SARS-CoV-2 BioID-based virus-host membrane protein interactome and virus peptide compendium: new proteomics resources for COVID-19 research. *bioRxiv* 2020.08.28.269175 (2020). doi:10.1101/2020.08.28.269175

28.   Samavarchi-Tehrani, P. *et al.* A SARS-CoV-2 – host proximity interactome. *bioRxiv* 2020.09.03.282103 (2020). doi:10.1101/2020.09.03.282103

29.   Gordon, D. E. *et al.* A SARS-CoV-2 protein interaction map reveals targets for drug repurposing. *Nature* **583**, 459–468 (2020).

30.   Nufer, O. *et al.* Role of cytoplasmic C-terminal amino acids of membrane proteins in ER export. *J. Cell Sci.* **115**, 619–628 (2002).

31.   Barlowe, C. Signals for COPII-dependent export from the ER: What's the ticket out? *Trends in Cell Biology* **13**, 295–300 (2003).

32.   Jimenez-Guardeño, J. M. *et al.* Identification of the Mechanisms Causing Reversion to Virulence in an Attenuated SARS-CoV for the Design of a Genetically Stable Vaccine. *PLoS Pathog.* **11**, e1005215 (2015).

33.   DeDiego, M. L. *et al.* A Severe Acute Respiratory Syndrome Coronavirus That Lacks the E Gene Is Attenuated In Vitro and In Vivo. *J. Virol.* **81**, 1701–1713 (2007).

34.   Carlton, J. G. & Martin-Serrano, J. Parallels between cytokinesis and retroviral

budding: A role for the ESCRT machinery. *Science (80-.).* **316**, 1908–1912 (2007).

35. Warren, S. C. *et al.* Rapid Global Fitting of Large Fluorescence Lifetime Imaging Microscopy Datasets. *PLoS One* **8**, 70687 (2013).

36. Cox, J. & Mann, M. MaxQuant enables high peptide identification rates, individualized p.p.b.-range mass accuracies and proteome-wide protein quantification. *Nat. Biotechnol.* **26**, 1367–1372 (2008).

37. Cox, J. *et al.* Andromeda: A peptide search engine integrated into the MaxQuant environment. *J. Proteome Res.* **10**, 1794–1805 (2011).

38. Tyanova, S. *et al.* The Perseus computational platform for comprehensive analysis of (prote)omics data. *Nature Methods* **13**, 731–740 (2016).

39. Mellacheruvu, D. *et al.* The CRAPome: A contaminant repository for affinity purification-mass spectrometry data. *Nat. Methods* **10**, 730–736 (2013).

40. Madeira, F. *et al.* The EMBL-EBI search and sequence analysis tools APIs in 2019. *Nucleic Acids Res.* **47**, W636–W641 (2019).

41. Waterhouse, A. M., Procter, J. B., Martin, D. M. A., Clamp, M. & Barton, G. J. Jalview Version 2-A multiple sequence alignment editor and analysis workbench. *Bioinformatics* **25**, 1189–1191 (2009).

42. Jeleń, F., Oleksy, A., Śmietana, K. & Otlewski, J. PDZ domains - Common players in the cell signaling. *Acta Biochimica Polonica* **50**, 985–1017 (2003).

Pearson et al., Figure 1

Pearson et al., Figure 2

A.

Pearson et al., Figure 3

A. Volcano plot: x-axis "Log₂ FC WT vs Cyto" ($\log_2$ FC WT vs Cyto) ranging from -10 to 12; y-axis "-log₁₀ p-value WT vs Cyto" ($-\log_{10}$ p-value WT vs Cyto). Labeled points: RPN2, BLZF1, GOSR2, RER1, SEC24B, VAMP3, ARFGAP2, RAB2A, RAB29, RAB6B, STAM, SCAMP3, GORASP2, TJP1, GOSR1, LMAN1, PALS1. Cyto (left), WT (right).

B. Western blots. Lanes: HaloTag, E-HT^Slick (Input); HaloTag, E-HT^Slick (Bound). Molecular weight markers: 95, 72, 55, 34, 25, 43. Antibodies: α-PALS1, α-GORASP2, α-RER1, α-HaloTag.

Pearson et al., Figure 4